2017

Photothermal imaging of PMMA film and photothermal spectroscopy of pHEMA hydrogel

BOSTON UNIVERSITY

COLLEGE OF ENGINEERING

Thesis

PHOTOTHERMAL IMAGING OF PMMA FILM AND PHOTOTHERMAL SPECTROSCOPY OF PHEMA HYDROGEL

by

DI HUANG

B.S., Fudan University, 2015

Submitted in partial fulfillment of the

requirements for the degree of

Master of Science

2017

Approved by

First Reader

Michelle Sander, Ph.D.
Assistant Professor of Electrical and Computer Engineering
Assistant Professor of Materials Science and Engineering

Second Reader

Shyamsunder Erramilli, Ph.D.
Professor of Physics

Third Reader

Lei Tian, Ph.D.
Assistant Professor of Electrical and Computer Engineering

DEDICATION

I would like to dedicate this work to my father and mother, Professor Michelle Sander, Atcha and my dearest friends who helped me in the past two years.

ACKNOWLEDGMENTS

I would like to thank my MS thesis advisor, professor Michelle Sander, for her guidance during my MS research and MS thesis writing. Would also thank professor Shyamsunder Erramilli for his valuable advices and professor Lei Tian for agreeing to be my thesis committee members.

I would like to thank Atcha Totachawattana for giving help to me on my MS research in photothermal spectroscopy and photothermal imaging. I would also thank her for her help during my MS thesis writing and thesis defense preparation.

I would like all the group members, including Ahmet Emin Akosman, Allison Marn, Jacky Zeng, Panagis Somalis, Casey Biederman, Karl Muench, Etienne Genier for their help during my MS research and my MS thesis defense preparation.

I would like to thank Professor Keith A. Brown and Le Li for fabrication of the PMMA USAF target sample. I would like to thank professor Allison Dennis and Margaret Chern for access to the vacuum oven. I would also thank professor Bjoern M. Reinhard and Min Xi for access to the electronic balance.

PHOTOTHERMAL IMAGING OF PMMA FILM AND

PHOTOTHERMAL SPECTROSCOPY OF PHEMA HYDROGEL

DI HUANG

ABSTRACT

The mid-infrared is a promising region for detection different materials. Many vibrational modes, including bending and stretching, are located in this regime. Photothermal spectroscopy and imaging in the mid-infrared region is an emerging new method for non-contact detection of molecular groups. Our approach to photothermal spectroscopy and imaging utilizes a near-infrared erbium doped fiber laser (EDFL) to detect the photothermal induced changes in the refractive index. These changes are excited by a mid-infrared quantum cascade laser (QCL) pump beam. The probe beam is detected by a commercially available near-infrared photodetector. This method has advantages of high sensitivity, label-free detection, high spatial resolution and high signal-to-noise ratio (SNR). Hydrogels such as pHEMA are polymers that are of interest for contact lens, drug delivery and soft tissue replacement. The pHEMA hydrogel can retain water content, causing the material to swell. Additionally, pHEMA has a critical temperature at which the hydrogel undergoes a glass transition. Photothermal spectroscopy of pHEMA is demonstrated in this thesis where the presence of this glass transition temperature can be revealed.

Additionally, photothermal imaging of a PMMA USAF target sample is shown and ideal parameters for high-resolution photothermal imaging are determined. In this

thesis, we report a spatial resolution much smaller than the diffraction limited spot size of the mid-infrared beam.

Key words: photothermal spectroscopy, photothermal imaging, pHEMA hydrogel, PMMA USAF target

TABLE OF CONTENTS

LIST OF TABLES

LIST OF FIGURES

LIST OF ABBREVIATIONS

DSC	Differential scanning calorimetry
EDFA	Erbium doped fiber amplifier
EDFL	Erbium doped fiber laser
FTIR	Fourier transform infrared spectroscopy
LCST	Lower critical solution temperature
pHEMA	Poly(2-hydroxyethyl methacrylate)
PMMA	Poly(methyl methacrylate)
PNIPAM	Poly(N-isopropylacrylamide)
PTS	Photothermal signal
QCL	Quantum cascade laser
wt	Water content

Chapter 1. Background

Photothermal spectroscopy is an emerging non-contact and label-free method for detection of organic compounds. In this thesis, the principle of photothermal spectroscopy and imaging are introduced. The properties of pHEMA hydrogels are introduced. The motivation of using photothermal spectroscopy and challenges it faces are introduced.

The background chapter is divided into five parts. In the first part, the mid-infrared "fingerprint" region is introduced. In the second part, the principle of mid-infrared spectroscopy is introduced. In the third part, photothermal imaging based on the combination of the photothermal spectroscopy and microscope is introduced. In the fourth part, a variety of thermal sensitive hydrogels are introduced. The pHEMA hydrogel and its glass transition properties are introduced as well. In the fifth part, advantages of photothermal spectroscopy and photothermal imaging are introduced.

1.1. Mid-infrared "fingerprint" region

The mid-infrared region is a promising regime for detection of different materials since many vibrational modes, including bending and stretching [6], are present in the mid-infrared region. Some of the mid-infrared absorption between 1000cm^{-1} to 1500cm^{-1} can be attributed to the molecular skeleton. This region is usually called the "fingerprint" region [6]. Mid-infrared spectroscopy is a useful tool for studying functional groups in different materials. It enables us to detect functional groups in different materials and distinguish the differences between different materials. Fig. 1 shows the vibrational frequencies of some common functional groups and bonds.

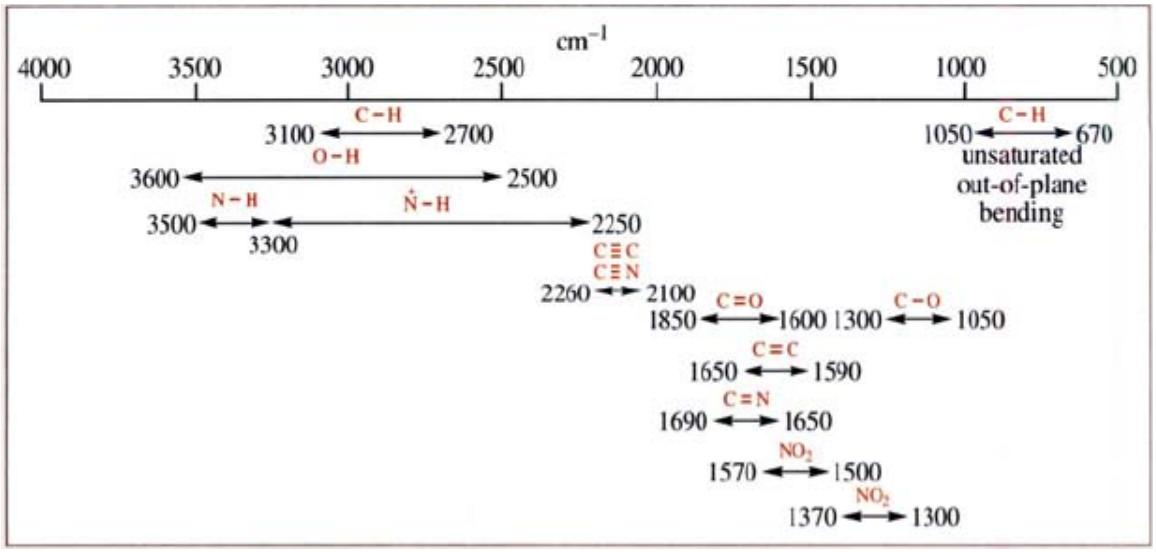

Fig. 1. Different vibrational frequencies for bonds and functional groups. The lines under the bonds or functional groups demonstrates the range in which these vibrational modes may be excited. Adapted from[6].

1.2. Mid-infrared photothermal spectroscopy

Mid-infrared photothermal spectroscopy is an indirect detection method based on the mid-infrared vibrational signatures of molecules. Instead of directly detecting the mid-infrared absorption spectrum by measuring the transmitted pump beam with a complex mid-infrared detector, which requires external cooling, photothermal spectroscopy utilizes a pump-probe mechanism. The photothermal lens effect is excited by the pulsed mid-infrared pump beam. The absorption of the mid-infrared pump beam induces a change in the sample temperature, resulting in a change the sample's refractive index. This change in refractive index can scatter or change the phase of the transmitted probe beam. In our experimental setup, the thermal-induced changes in the refractive index can be detected by a near-infrared probe beam that spatially overlaps the pump beam at the sample [8–9]. The near-infrared probe beam is measured by a commercially

available near-infrared photodetector. The photothermal signal is extracted from the periodical modulation of the probe beam. Photothermal spectroscopy enables mid-infrared detection with high signal to baseline contrast [10] and can have applications in detection of large categories of chemicals [9].

Photothermal spectroscopy has been demonstrated for the detection of single molecules [2], single nanoparticles [3], and biological samples [4]. Recently, the development of high brightness quantum cascade lasers (QCL) in mid-infrared region, which brightness exceeds that of globar sources or thermal sources (typically used in FTIR), enables photothermal spectroscopy to be performed in the mid-infrared region [5].

1.3 Photothermal imaging

Photothermal imaging in the mid-infrared region enables highly sensitive, label-free imaging by utilizing the different absorption wavenumbers for different function groups in mid-infrared region. With the development of quantum cascade lasers (QCLs), mid-infrared imaging can be achieved [11].

By combining photothermal spectroscopy and microscopy, photothermal imaging of chemical samples can be achieved in mid-infrared region [12–13]. By tuning the mid-infrared pump beam to the absorption peak of various function groups, photothermal imaging can be achieved by using a confocal geometry and raster scanning mechanism. With a near-infrared probe beam whose wavelength is shorter than that of the mid-infrared pump beam, photothermal imaging can achieve higher spatial resolution than the

diffraction limited spot size of the mid-infrared beam [13]. Photothermal imaging in the mid-infrared region has been applied in living cell imaging [14] and single particle detection [15].

1.4. Properties of thermally sensitive polymer

Stimuli-responsive polymers or "smart polymer materials", are of interest because they can be manipulated by external stimuli, such as temperature, pH and salt concentration. Some polymers have an interesting temperature response. For example, poly(N-isopropylacrylamide) (PNIPAM), can undergo a hydrophilic–hydrophobic transition at a "lower critical solution temperature" (LCST) of about 32 °C [16]. When the temperature is above the LSCT, the polymer will become less hydrophilic, resulting in expulsion of water in the polymer and collapsing of the polymer [17].

Other temperature sensitive polymers such as hydrogels, including poly(2-hydroxyethyl methacrylate) (pHEMA), are of interest due to their varieties of applications including uses in contact lens [18], drug delivery [19] and soft tissue replacement [20]. The pHEMA hydrogel has a glass transition temperature. Above this temperature, the polymer will turn from glassy like into a viscous or rubbery state. The glass transition temperature decreases when the hydrogel water content goes up, as shown in fig. 2 [21]. The macromolecular properties in pHEMA are characterized by non-covalent interactions of hydrogen-bonds among the polymer chains as well as the hydrated water molecules [22]. Differential scanning calorimetry (DSC) study are shown

in fig. 3 for a pHEMA hydrogel with a water content of 8%. The step in the baseline is assigned as glass transition [23]. The DSC trace drops down at the vicinity of the glass transition temperature demonstrates that the sample thermal capacity increases when the hydrogel is above glass transition temperature. The DSC curve dip at glass transition temperature indicates that the hydrogel structure changes (close to melting) at the glass transition temperature. Fig. 4 shows an FTIR spectrum of the pHEMA hydrogel [27]. There is an absorption peak around 1730cm^{-1}, which consists of C=O stretching mode absorption peak at 1730cm^{-1} and hydrogen bonded C=O with OH stretching mode absorption peak at 1703cm^{-1} [25]. The mid-infrared absorption at around 1730cm^{-1} and the glass transition properties shows pHEMA hydrogel is a promising material for photothermal spectroscopy studies.

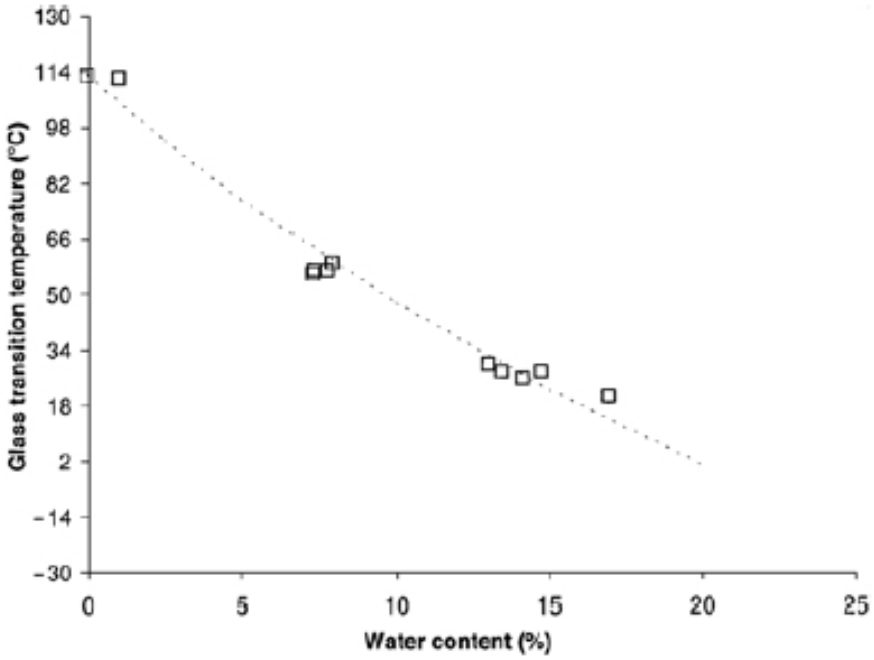

Fig. 2 The relationship between pHEMA water content and the glass transition temperature. The water content is defined as the percent of water weight in the total hydrogel weight. Our photothermal experiment focuses on pHEMA samples with a water content between 10% and 15%. This figure is adapted from [21].

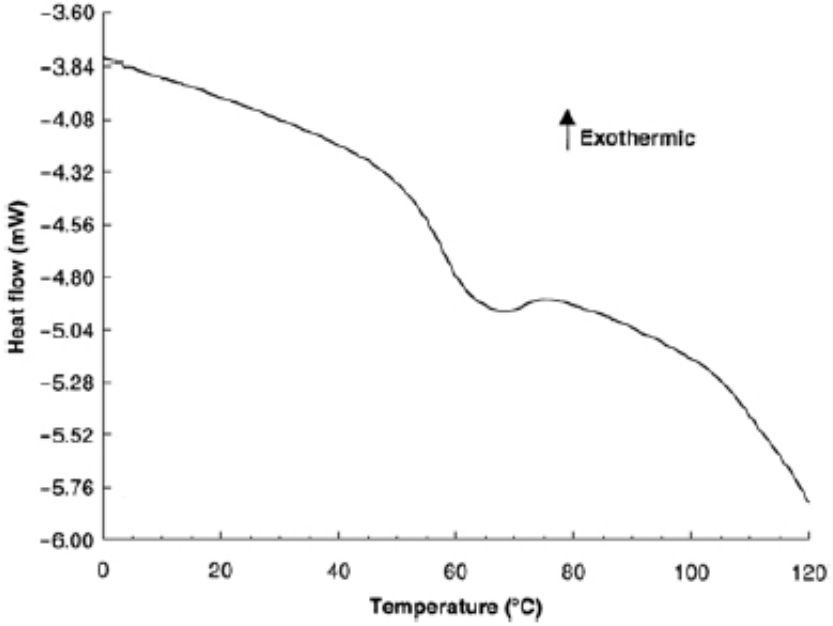

Fig. 3 DSC analysis of pHEMA hydrogel. The pHEMA hydrogel has a water content of 8% for this sample The step in the baseline is assigned as glass transition. The DSC trace drops down in the vicinity of the glass transition temperature, which means that the thermal capacity increases above the glass transition temperature. The DSC trace's dip at glass transition temperature implies there might be a hydrogel structure changes. This figure is adapted from [21].

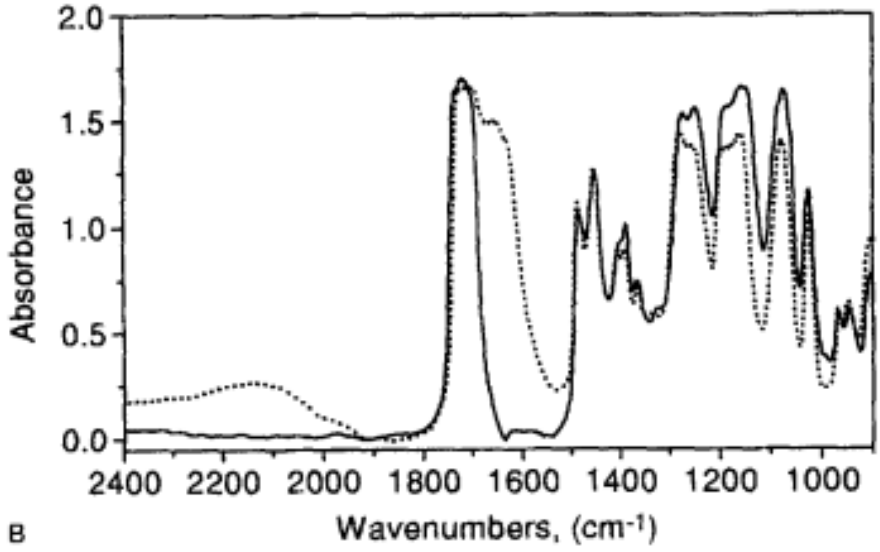

Fig. 4 FTIR spectrum of pHEMA shows an absorption peak at around 1730cm^{-1} for different water content levels. The absorption peak consists of the free C=O absorption at 1730cm^{-1} and C=O---OH hydrogen bond absorption at 1703cm^{-1} [25]. The dashed and solid lines represent the spectrum for pHEMA with a water content of 38% and 2.6%, respectively. This figure is adapted from [27].

1.5. Motivation

Spectroscopy and imaging in the mid-infrared region are interesting due to the large number of characteristic vibration modes in this region, and each mode will have a mid-infrared absorption if it involves a dipole moment change [6]. The high absorption cross section (usually 10^{10} times higher) [10] compared to the scattering cross section (utilized in Raman spectroscopy) enables mid-infrared spectroscopy to be applied for highly sensitive detection or detection of low concentrations. It gives an interesting and useful way of detecting and studying different materials in the mid-infrared region.

The near-infrared probe beam is generated by an erbium doped fiber laser (EDFL) in our photothermal system. The near-infrared wavelength is tuned to minimize sample absorption of the probe beam as well as to minimize water vapor absorption in the near-infrared region. The near-infrared probe beam can be easily amplified by using additional erbium doped fiber amplifiers (EDFAs). By focusing the near-infrared beam, the system can achieve much higher spatial resolution than diffraction limited spot size of mid-infrared beam.

The photothermal spectroscopy system also faces some challenges. Firstly, the pump-probe mechanism integrates two different wavelengths into the system. Thus all the optics must be suitable for both the pump and probe beams. Secondly, photothermal spectroscopy requires a spatial overlap between the pump induced thermal lens area and probe beam at the sample in order to detect the photothermal signal. Thus, a high quality optical alignment is required. Thirdly, the objective lens has chromatic aberration. Both beams are focused to achieve the high spectral sensitivity and high spatial resolution but

the sample plane location can vary slightly. Fourthly, material absorption in the near-infrared region might jeopardize the probe beam detection. Hence, the near-infrared beam wavelength must be selected to avoid both liquid water absorption in hydrogel samples and material absorption.

In this thesis, by using photothermal spectroscopy, the aim is to characterize the mid-infrared photothermal spectrum of a pHEMA hydrogel. This is the first time that hydrogels will be studied with photothermal methods. By increasing the QCL output, we will study the glass transition properties of the pHEMA hydrogel to provide a novel characterization method of this regime. With a PMMA USAF target, we will determine the best spatial resolution of the photothermal imaging system and show sub-diffraction limited resolution. By comparing both photothermal images and the quantitative analysis of them, the best parameter for photothermal imaging will be determined.

Chapter 2. Experimental details

2.1. Photothermal spectroscopy system

Our photothermal spectroscopy system utilizes an erbium doped fiber probe laser (EDFL) and a tunable high brightness QCL pump laser for label-free and highly sensitive detection. The experiment set up schematic diagram is shown in fig. 5. The near-infrared beam is guided from the optical fiber to free space by using a collimator. The near-infrared probe beam and the mid-infrared pump beam are combined with a dichroic mirror. The two beams are co-aligned and then focused onto the sample by a ZnSe objective lens (numerical aperture = 0.25, focal lengths = 6mm). The diffraction limit spot size of the beam is calculated by using equation (1), the minimum spot diameter of mid-infrared beam is about 12μm, and the minimum spot diameter of the near-infrared beam is around 3μm. The optical component after the sample is designed for the near-infrared probe beam, the mid-infrared probe beam is filtered, and only the near infrared beam passes through the detection arm. The probe beam is detected by the InGaAs photodetector (ET3000A, EOTech). A voltage pre-amplifier (SRS 560, Stanford Research Systems) amplifies the output signal at 200 times between 10kHZ to 1MHz. The lock-in amplifier (HF2LI, Zurich Instruments) is synchronized to the pump repetition rate to extract the photothermal signal from the periodical modulation of near-infrared probe beam. The photothermal signal is defined as the modulated scatter of the near-infrared probe beam.

$$d = \frac{\lambda}{2 \times N.A} \tag{1}$$

A pulsed QCL (model 41060, Daylight Solutions) is used to generate the mid-infrared pump laser beam between 1575cm^{-1} and 1745cm^{-1}. By tuning the mid-infrared laser wavenumber across the sample absorption band, the photothermal spectrum can be obtained. The QCL has a repetition rate of 100kHz, a pulse duration of 500ns and a duty cycle of 5%. The QCL output power is controlled by using different QCL drive current. The probe beam has an output centered at 1606nm with a full width half maximum (FWHM) of 0.85nm. The maximum near-infrared probe beam power after the collimator is measured to be 38.03mW. After the free space optics, the maximum probe power focused at the sample position is 1.55 mW and 0.974mW of probe power is focused onto the photodetector.

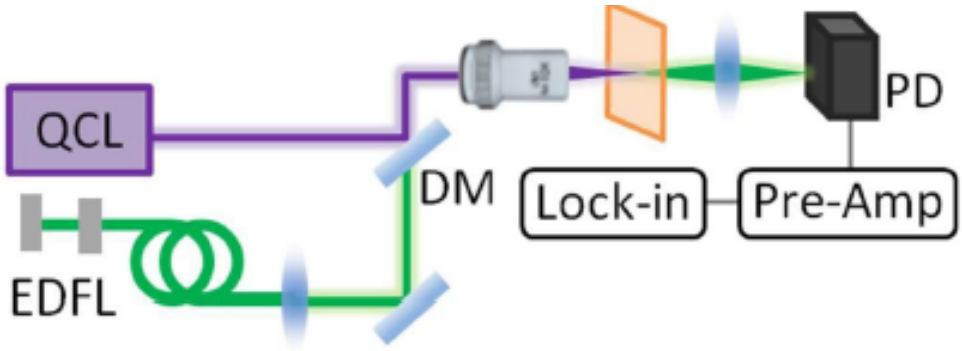

Fig. 5. The schematic diagram of the photothermal spectroscopy system. The pump beam is generated by a quantum cascade laser (QCL), the probe beam is generated by an erbium doped fiber laser (EDFL) and amplified by an erbium doped fiber amplifier (EDFA). The two beams are combined at the dichroic mirror and are co-aligned to pass through the sample. Only the near-infrared probe beam is detected by the photodetector (PD). The pre-amplifier (Pre-Amp) and lock-in amplifier (Lock-in) are used to extract the photothermal signal from the periodically modulated near-infrared probe beam. The figure is adapted from reference [10].

When measuring the photothermal spectrum, the whole system is purged in a sealed chamber. Dry air is pumped into the chamber to decrease the humidity, thus to minimize the influence of mid-infrared water vapor absorption on the photothermal

spectrum. When taking the photothermal measurement, the humidity in the chamber is below 0.5%.

With a raster scanning approach, the photothermal spectroscopy system can perform label-free imaging in the mid-infrared region. The scanning is realized by moving the sample along x or y direction. The sample x,y and z movements are performed by the xyz platform, with a minimum step size of 1μm. The platform is controlled by Labview programs. The relative xy position is monitored by the program to help locating the sample. Movements along each xy and z direction are controlled independently by the xy scanning and z scanning Labview programs accordingly. The xy movement can be manually controlled by the joystick and z position can be manually controlled by the knob.

2.2. Other experiment facilities

The mid-infrared absorption spectrum is measured by Fourier transform infrared spectroscopy (FTIR) (NEXUS 870, Thermo Nicolet) in the basement lab. The wavenumber resolution is $1cm^{-1}$ and the each mid-infrared spectrum is the average of 64 measurements. The sample is manually adjusted to reach the focal spot of the mid-infrared beam by using a red guide laser, the gain is set to 1 and the aperture is set to 7. The mid-infrared spectrum is taken between $1000cm^{-1}$ to $4000cm^{-1}$. Since the sample thickness is not uniform over the whole sample, the mid-infrared absorption spectrum of the sample is calculated by averaging four FTIR spectra taken at four different sample

positions to represent the absorption spectrum of the whole sample.

The sample weight is measured by an electronic balance (AE240, METTLER TOLDEO) in basement lab, too. The minimum weight resolution is 0.1mg for the 20g range mode. The sample is measured in a closed chamber to avoid the flowing air or vibration perturbations. The sample weight is calculated by the average of three measurements each time.

The sample temperature is controlled by a chiller (RTE-211, Thermo Neslab). The bath fluid is water. The highest allowed temperature for our system is 55ºC. The chiller's temperature represents the bath fluid temperature. The accurate sample temperature is different from the bath fluid temperature. The actual temperature of the sample is measured by a thermometer (PM20700, Thermolyne) directly from the CaF_2 windows. The corresponding sample temperature versus chiller temperature relationship is used to determine the accurate sample temperature by using the chiller temperature.

The optical imaging of the PMMA USAF target sample is taken from the Nikon microscopy system (Optiphot LV150) at 8^{th} floor in PHO. Optical and photothermal images of the PMMA USAF target sample are compared.

2.3. Overview of Sample selection

The prospect sample should qualify the following properties for our photothermal spectroscopy system. Firstly, the target sample should have an absorption peak in the QCL range (from 1580cm^{-1} to 1740cm^{-1}). Secondly, if the sample has around 0.6 O.D. absorbance at the absorption peak, then we should get adequate thermal effects for the

photothermal lens effects. Thirdly, the substrate medium should minimize the thermal lens effect so that it won't interfere the photothermal measurement of the sample. The sample should also have low absorbance in the near-infrared region at the probe beam wavelength. For hydrogel samples containing water, the sample absorption peak should be away from the liquid water absorption peak at 1630cm^{-1}.

2.4. The pHEMA sample

The pHEMA hydrogel is a temperature sensitive hydrogel that we applied in our photothermal study. The pHEMA crystal instead of the HEMA solution is chosen because HEMA has strong near-infrared absorption at the near-infrared probe beam wavelength 1606nm and the absorption peak decreases after polymerization [23]. The pHEMA crystal (Mv 300,000) is purchased from Sigmaaldrich. The pHEMA sample is prepared with pHEMA solution. The pHEMA solution is prepared by dissolving 0.1g of pHEMA crystal in 2.0mL methanol. 100μL of pHEMA solution is pipetted onto the 1mm thick CaF_2 window to form a thin layer. The sample is put in the oven at 70ºC for at least 12 hours to evaporate all methanol content. Then the sample is put in the oven at 150ºC for 1 hour to evaporate all the water content in the sample. Then the sample weight is measured as the mass of dry pHEMA. The dry pHEMA mass is used to calculated the sample water content. The dry pHEMA is soaked into distilled water for at least 7 days to ensure the pHEMA hydrogel is fully saturated. The resulting hydrogel is then sandwiched with another 1mm thick CaF_2 window to prepare the sample. It takes around 4 days for

the sample water content to drop to around 15%. The water content (wt) is defined by equation (2):

$$wt\% = \frac{m_{pHEMA} - m_{drypHEMA}}{m_{pHEMA}} \times 100\% \quad (2)$$

Then the sample is placed into the copper sample mount with the chiller connected to it. The vacuum grease is applied to the caps rings to seal the sample to slow down the dehydrating of the pHEMA hydrogel. The overall sample temperature is measured directly on the CaF_2 window by using the thermometer.

For our photothermal spectroscopy, calculating the temperature changes induced by the QCL pump beam absorption is a very important. The QCL pump beam induced local temperature change can be calculated based on the following assumptions: (1) The change in pHEMA temperature is induced individually by each pulse; (2) The mid-infrared pump beam only heats the area within the QCL beam waist on the sample; (3) All the mid-infrared beam power absorbed will convert to heat. Changes in local temperature can be calculated using the following equation (3):

$$\Delta T = \frac{(1 - e^{-\alpha}) \cdot E_{pulse}}{C_{pHEMA} \cdot \pi \cdot r_w^2 \cdot z \cdot \rho_{pHEMA}} \quad (3)$$

α is the pump beam absorbance, z is the thickness of the sample, C_{pHEMA}=0.2J/g.K is the thermal capacity of the pHEMA [26]. E_{pulse} is the pulse energy for each pulse, ϱ_{pHEMA}=1.15g/cm^3 is the density of pHEMA. r_w is the radius of the Gaussian beam (e^{-2}). The diffraction limit spot size radius can be calculated by equation (4)

$$r_w = \frac{\lambda}{4 \times N.A} \tag{4}$$

For our photothermal system, the numerical aperture is 0.25. The beam radius is 11.5μm. The sample thickness is calculated the sample weight divided by pHEMA density and sample area.

2.5. PMMA USAF target sample

The 1951 USAF resolution test chart is a resolution test pattern conforming to MIL-STD-150A standard, set by the US Air Force in 1951. It is still widely accepted to test the resolving power of imaging systems such as microscopes and image scanners. The sample is fabricated by spin coating a 330nm layer of polymethylmethacrylate (PMMA) onto a 1mm thick CaF_2 window. The USAF resolution test pattern is etched into the PMMA by electron beam lithography using a Zeiss Supra 55 scanning electron microscope. The PMMA is removed from the pattern area while a PMMA film remains on the other area of the substrate. It creates a negative contrast.

The USAF target has groups of line bars, and the largest line bars that the imaging system cannot resolve is the limitation of resolving power. In our photothermal imaging system, the smallest resolvable lines pairs are determined by both pattern imaging and photothermal signal line scan analysis according to Rayleigh criterion.

Chapter 3. Experiment results

3.1. FTIR spectrum of pHEMA hydrogel

Two sets of pHEMA hydrogel sample are prepared for the experiment. Sample 1 has a dry pHEMA mass of 0.0050g and 10±2% water content. Sample 2 has a dry pHEMA mass of 0.0052g and 15±2% water content (total sample mass equals to 0.0061g). Since the pHEMA sample thickness is not uniform for the whole sample. FTIR spectrum is calculated by averaging the four measurements at different positions to represent the whole sample. The FTIR spectra are shown in fig. 6. The sample FTIR spectrum shape for the same water content and different sample temperatures are the same. The absorbance difference is within the uncertainty of the measurement at around the absorption peak. It means that the mid-infrared absorbance changes due to temperature changes are negligible. Beside, the linear mid-infrared absorption spectrum when the sample temperatures are below and above glass transition temperature are negligible.

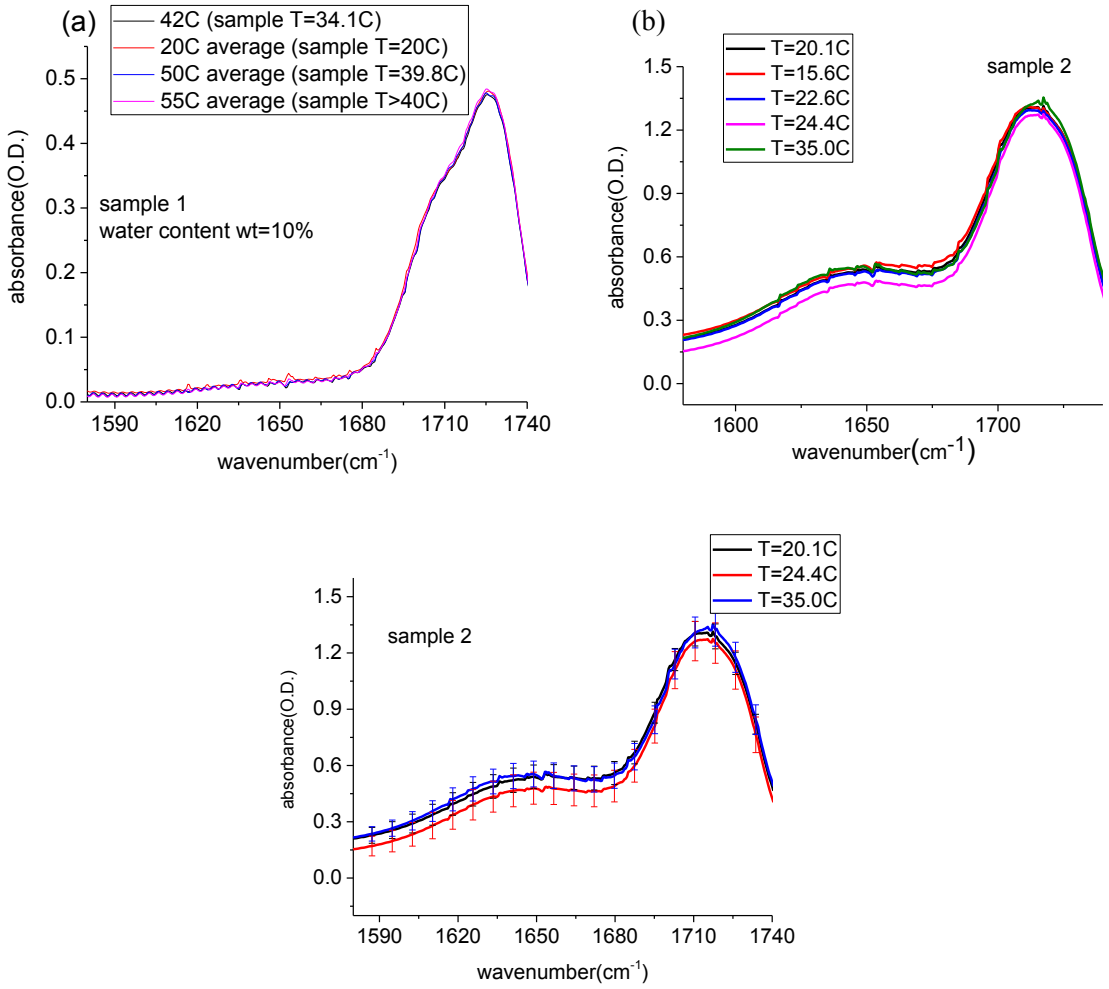

Fig. 6 FTIR spectrum at different temperatures for (a) sample 1, water content wt=10±2% and (b) sample 2, water content wt=15±2%. The spectrum shape doesn't change with temperature. (c) shows the absorbance changes between T=20.1C, T=24.4C and T=35.0C fall within the absorbance measurement error at around the absorption peak between 1640cm-1 to 1740cm-1. It means that the absorbance changes due to temperature changes is negligible at around the absorption peak.

Fig. 7 shows the comparison between the QCL gain spectrum normalized photothermal spectrum and the normalized FTIR spectrum of sample 2. Fig. 7(a) shows the photothermal spectrum taken at sample temperature of 20.1ºC and a QCL drive current of 500mA. Fig. 7(b) shows the FTIR spectrum taken at sample temperature of

20.1ºC before the photothermal spectra were acquired. Both spectra share the same peak centered around 1712cm^{-1}. The photothermal spectrum is normalized by dividing the QCL gain spectrum at a QCL drive current of 500mA to offset the photothermal spectrum shape changes due to the QCL output. The FTIR spectrum and the photothermal spectrum peak strength are normalized to 1 so that both spectra can be easily compared. Both normalized photothermal spectrum and normalized FTIR spectrum share the same peak position at 1712cm^{-1} showing a good agreement between both measurement instruments.

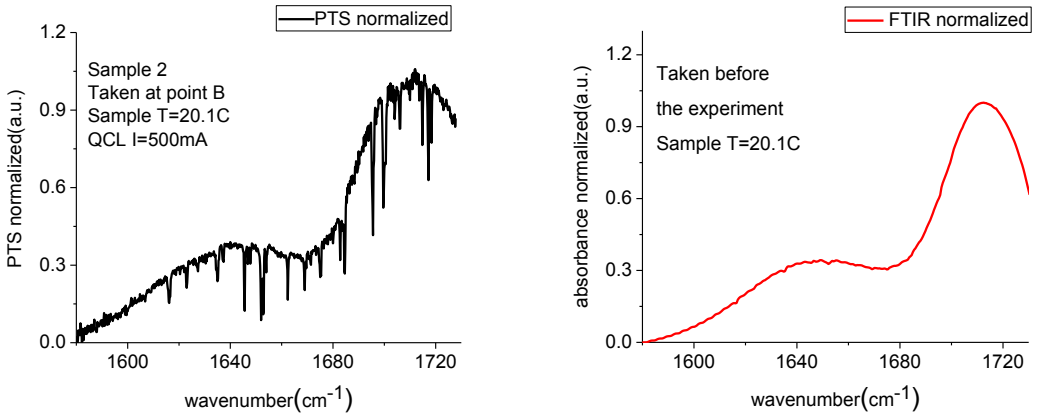

Fig. 7 The comparison between the gain spectrum normalized photothermal spectrum and the normalized FTIR spectrum. (a) is the gain spectrum normalized photothermal spectrum taken at sample temperature T=20.1ºC, QCL drive current=500mA and (b) is the normalized FTIR spectrum taken at sample temperature T=20.1ºC before the experiment. Both spectrum are normalized to 1. Both spectrum share the same peak at around 1712cm^{-1}.

3.2. Photothermal spectrum of pHEMA hydrogel

The photothermal spectrum is measured in a purged chamber. The chiller is set to 20.0ºC to keep the sample temperature steady. For sample 2 (total sample mass 0.0061g,

water content wt%=15±2%), a scan along the z axis is recorded at a QCL current of 500mA, at 1728cm^{-1} to find the z position with the highest photothermal signal. The experiment z position is set to be the z position with highest photothermal signal (PTS). Photothermal spectra are taken at reference point 1,2 and 3 as a baseline for reference after each group of experiment. The data recorded at point A and point B are 500μm away from z scanning point and reference point to make sure the measurement at point A and B does affect the reference point. The relative positions of different points are shown in fig. 8.

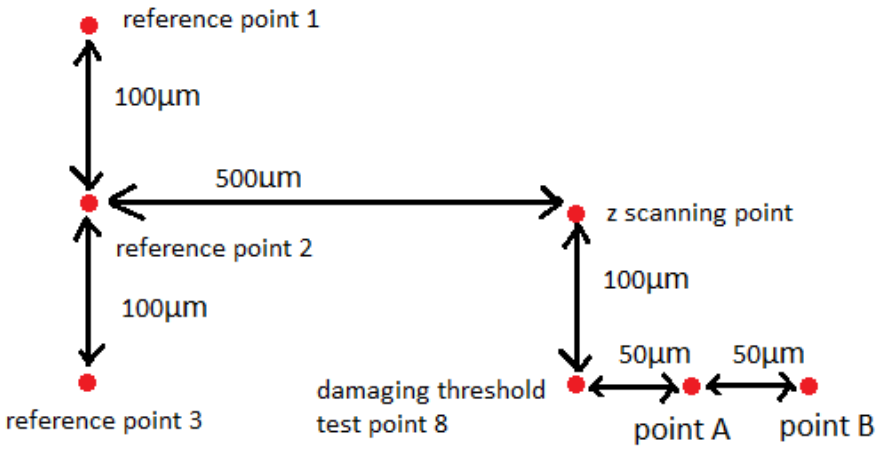

Fig. 8. The relative positions of different points on the pHEMA hydrogel sample. The point A, point B and damaging threshold test point are at least 500μm away from the reference point 1,2 and 3 to make sure measurements at these points doesn't interfere each others.

Thermal damaging threshold of sample 2 is measured at damaging test point before the experiment. The sample damaging is defined as photothermal spectrum shape or strength changes after each group of experiments compared to reference measurements at a QCL drive current of 500 mA. The damage threshold is defined as the highest QCL drive current that will not damage the hydrogel sample if the QCL beam at

1728cm^{-1} illuminated the sample for an hour and photothermal spectra are taken several times. From fig. 9(a)–(d), it can be observed that sample damage occurs at 650mA but not at 600mA. It means that the sample damage threshold is 600mA.

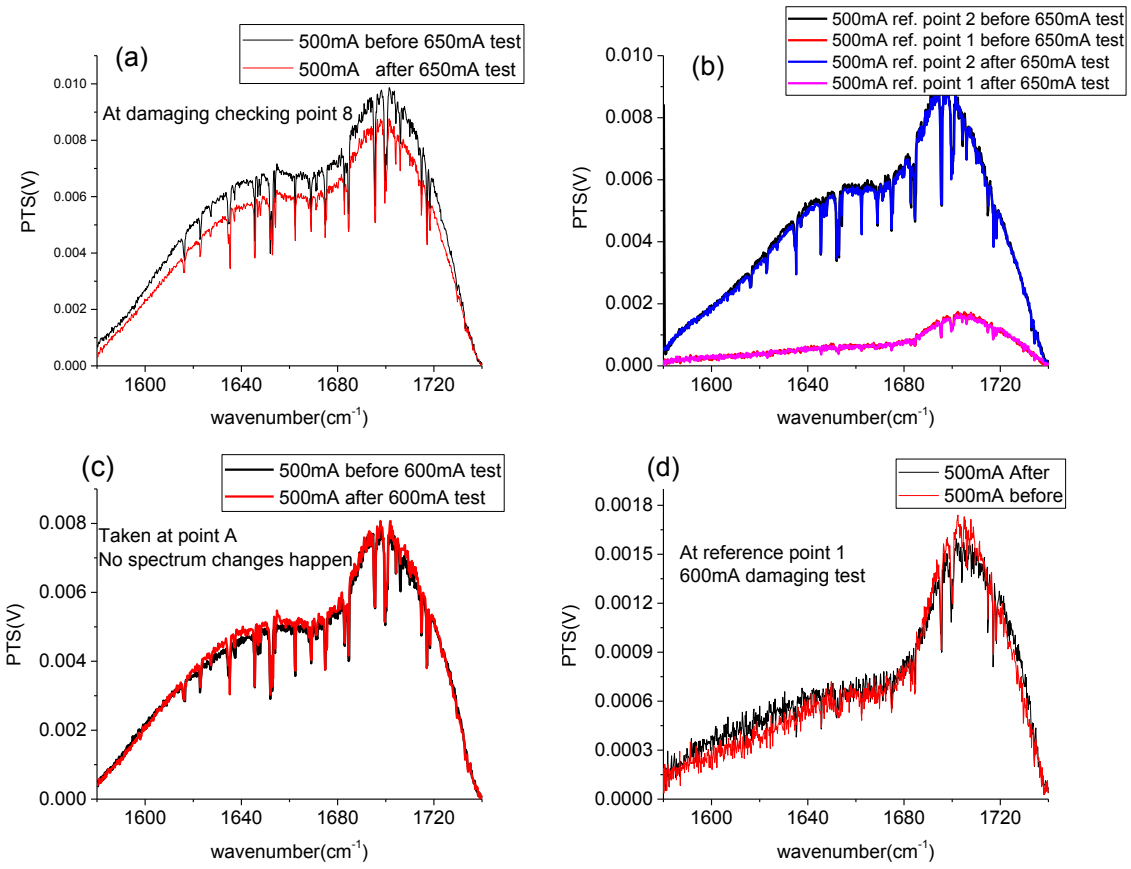

Fig. 9. Damage threshold testing. (a) shows a change in spectral shape at 500mA before and after recording a spectrum at QCL drive current=650mA. This means that 650mA is above the damage threshold. (b) Comparison of the spectrum at reference point indicates spectrum changes at point 8 is not due to sample overall changes. (c) There is no spectrum changes at 500mA before and after 600mA testing at point A, it means there is no sample damaging. (d) verifies there is no overall sample spectrum changes happens.

Table 1. Chiller temperature and corresponding sample temperature relationship. This group of data is taken at room temperature T=20.6ºC

Chiller temperature/^{o}C	Sample temperature/^{o}C	Chiller temperature/^{o}C
10	15.6	10
15	17.8	15
20	20.1	20
25	22.6	25
30	24.4	30
50	35.0	50

The chiller temperature and corresponding sample temperature relationship is shown in table 1. The chiller is set to 10ºC and 20ºC successively, photothermal spectrums are taken at point A with the QCL drive current varies from 400mA to 600mA. The photothermal signal versus QCL drive current curves at around 1728cm^{-1} free C=O stretching absorption line at different sample temperatures are shown in fig. 10(a) and(b). The photothermal signal in fig. 10(a) and (b) is calculated by averaging the photothermal signal at 1727cm^{-1}, 1728cm^{-1} and 1729cm^{-1}. Fig. 10(c) and (d) shows the photothermal signal curve at 1702cm^{-1}, near the hydrogen bonded C=O with OH absorption line. These curves show the same trend that the photothermal signal increases linearly with an increase in the QCL drive current. After a threshold QCL drive current, the photothermal signal curve slope drops down. The turning point is defined as the point that photothermal signal curve slope drops down. The critical current is defined as the QCL drive current at the turning point. The turning point is determined by the intersection of the two red dash line, the dash line parameter is calculated by linear fitting. Critical currents vary with different sample temperatures. The higher the sample temperature is, the lower the critical QCL drive current is. Fig. 10(e) and (f) show that there are no

spectrum changes at QCL drive current=500mA after the experiment. It means no sample damage happens while measurements are conducted.

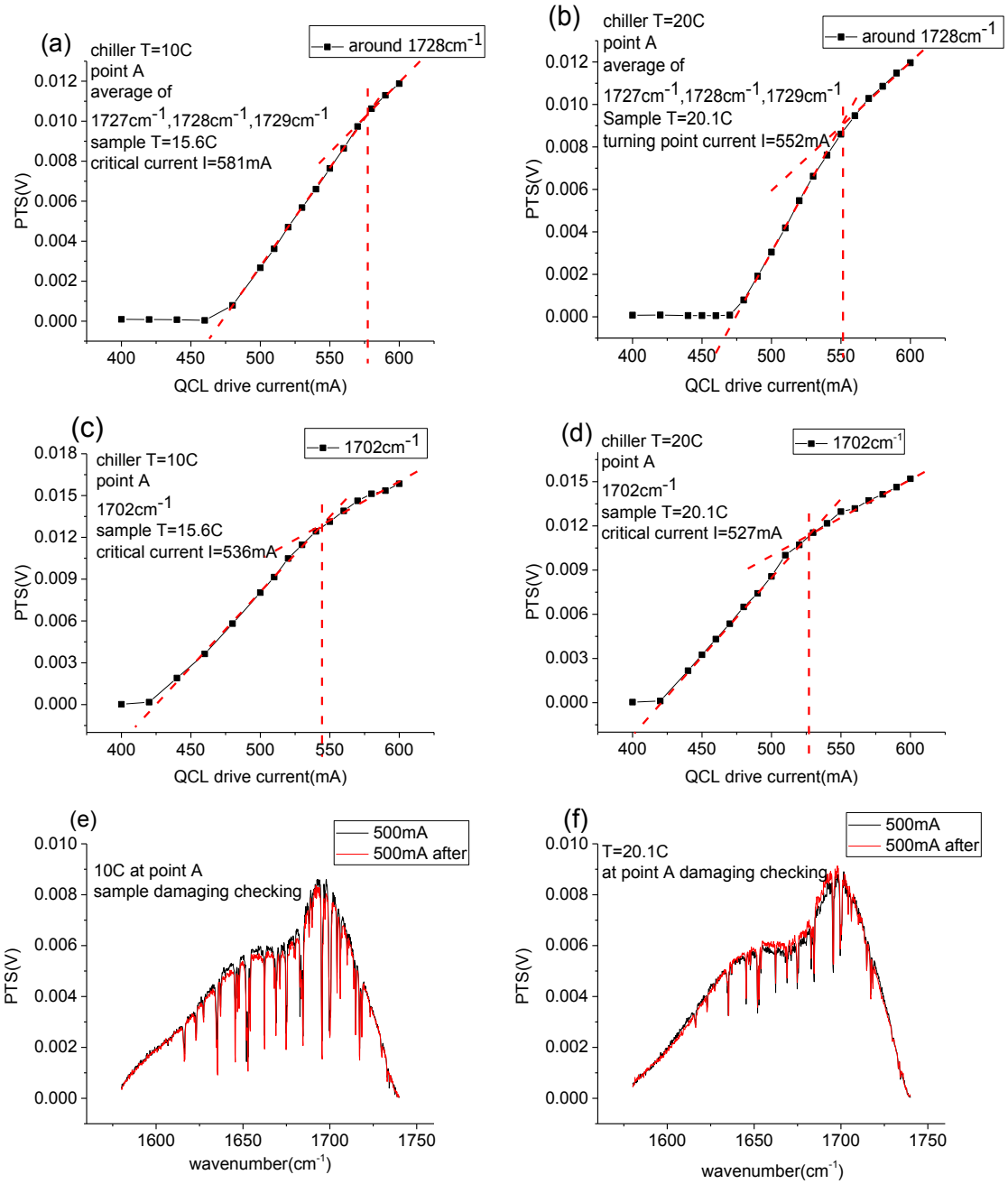

Fig. 10. The QCL drive current and photothermal signal relationship curve. (a) and (b) are taken at around 1728cm^{-1}, (a) has a critical current of 581mA. (b) has a critical current of 552mA. (c) and (d) are taken at 1702cm^{-1}. (c) has a critical current of 536mA. (d) has a critical current of 527mA. For (a) and (b), (c) and (d), the higher sample temperature has lower critical current. (e)

and (f) shows the spectrum doesn't change at 500mA during and after the measurement. It means that the sample has not been damaged. Photothermal signal changes doesn't due to sample damage.

Another group of data is taken at point B. The chiller is set to 25C, 10C, 20C, 50C, 30C successively. Repeat the same data taking process at point A. The QCL drive current and photothermal signal curves at around 1728cm^{-1} are shown in Fig. 11(a)–(d). It shows the same trend that QCL drive current at turning point goes down when the sample temperature goes up. Fig 11(e) shows when chiller is set to 50.0ºC(sample temperature T=35.0ºC), photothermal signal is linearly increasing with QCL drive current. Fig. 11(f) shows a linear fitting of the critical current and sample temperature. It shows a linear relationship between the critical current and the sample temperature from 10ºC to 30ºC. Fig. 11(g)–(k) shows the comparison of spectrums taken at 500mA during and after the experiment. The spectrum doesn't change after the experiment. It indicates that no sample damaging happens during measurements. The QCL drive current and photothermal signal don't change due to sample damaging. Fig. 11(l) shows the photothermal spectrum below and above the critical current. Here, the raw photothermal spectrum is adjusted by normalizing it with the QCL gain curve spectrum. This takes into account that for a given QCL drive current the power varies at different wavenumbers so that a comparison with the FTIR spectrum can be made.

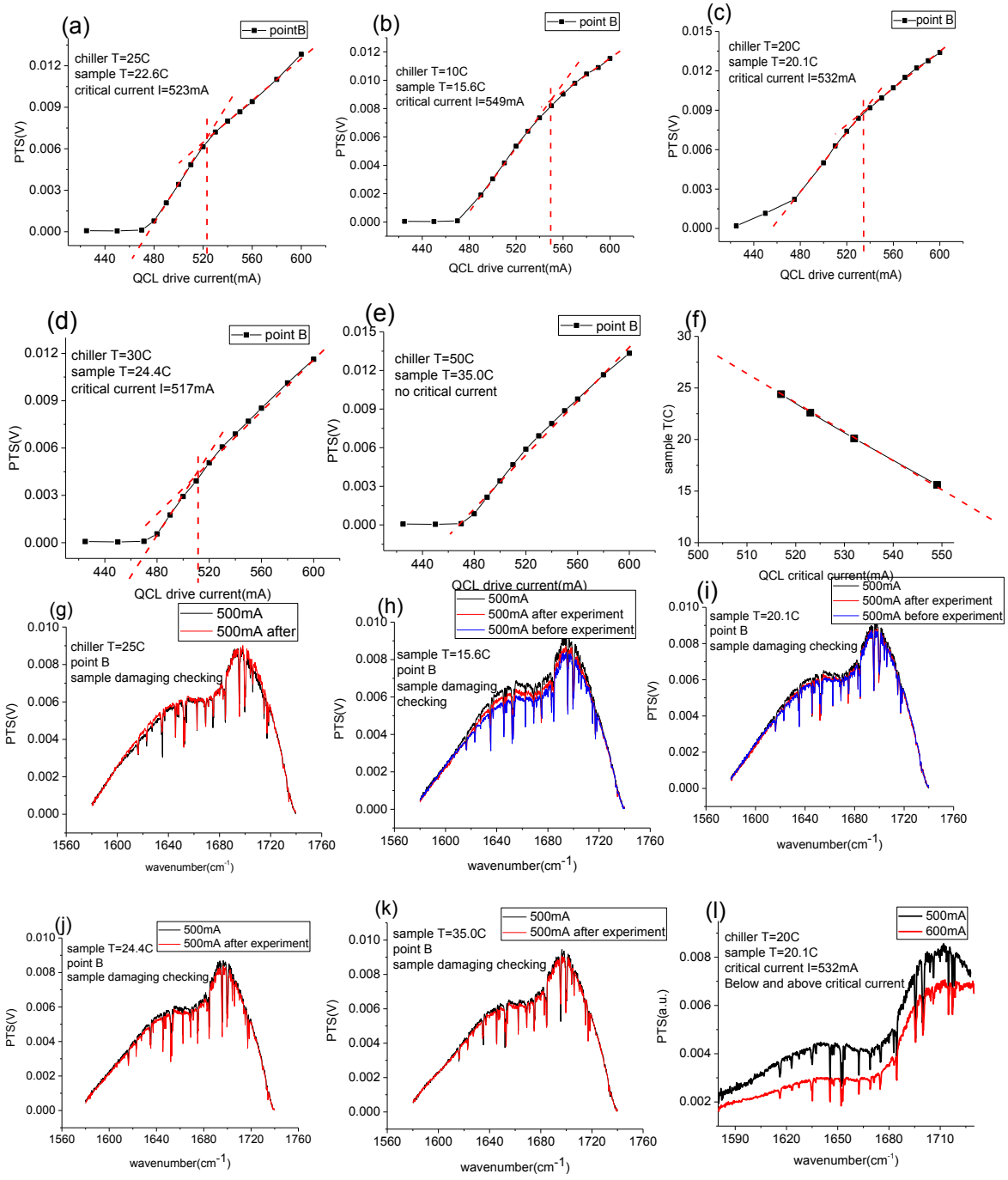

Fig. 11. (a)-(e) is the QCL drive current and photothermal signal relationship curves taken around 1728cm^{-1}, the data is obtained by averaging data at 1727cm^{-1}, 1728cm^{-1},1729cm^{-1}. (a)-(d) has a critical current of (a) 523mA; (b) 549mA; (c) 532mA; (d) 517mA. There is no turning point in (e). (f) shows a linear relationship between QCL drive current I and sample temperature T. (g) to (k) shows there is no spectrum changes at QCL drive current=500mA after the experiment. It means that there is no sample damaging happens.(l) shows the photothermal spectrum below and

above the critical current at sample T=20.1C at point B, the photothermal spectrum is divided by the QCL gain spectrum to offset the spectrum shape changes induced by the QCL output.

The QCL output power versus QCL drive current curve is measured by a thermal power meter at sample plane. The curve at 1702cm^{-1} and 1728cm^{-1} is shown in fig. 12. It can be seen that above lasing threshold, the QCL output power at 1702cm^{-1} and 1728cm^{-1} increased linearly with the increase of QCL drive current. The laser threshold current is calculated to be the intersection of the baseline and the linear fitting of the slope. The baseline is calculated by averaging the QCL output power from 400mA to 450mA. The baseline is 0.1292mW and the laser threshold current is 431mA for 1702cm^{-1} and 480mA for 1728cm^{-1}.

The linear relationship between the QCL drive current and QCL output power above threshold implies that the slope changes of shows in fig. 10 and fig. 11 cannot be attributed to the QCL output.

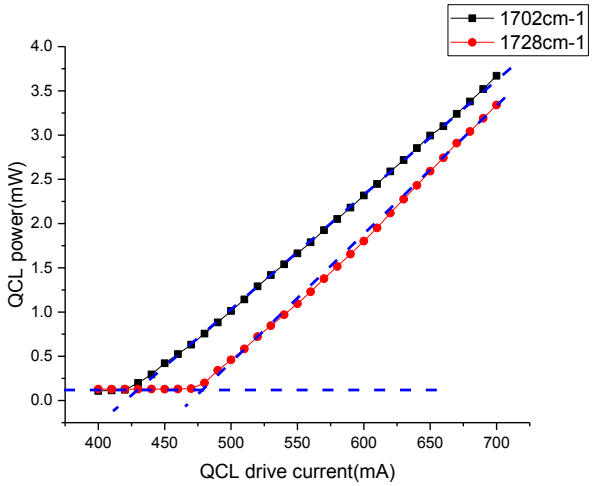

Fig. 12 The relationship between QCL drive current and QCL output power. The QCL output power above lasing threshold at 1702cm^{-1} and 1728cm^{-1} increase linearly with an increase in the QCL drive current. This demonstrates that photothermal signal slope changes are not due to QCL output.

The most possible explanation for this photothermal signal slope changes is due to pHEMA hydrogel glass transition happens at the vicinity of the glass transition temperature. The water content of pHEMA hydrogel sample 2 is 15±2%, the glass transition temperature is 9~34ºC accordingly [21]. Firstly, the QCL drive current at the turning point and the sample temperature have a linear relationship; the QCL output power linearly increases with the QCL drive current; the sample temperature is rising linearly with increasing QCL output power. It means that the photothermal signal and QCL drive current curve's slope change happens at a fixed sample temperature. Secondly, according to the linear fitting from fig.10(f), when the critical current is equal to 480mA (1728cm^{-1} lasing threshold, which means no QCL output power), the sample temperature equals to 34ºC, it is at specific temperatures that slope changes happens. And it is within the range of glass transition temperature at 15±2% water content, which is corresponding to 9~34C [21]. Thirdly, according to the DSC trace shows in fig.3, there is an increase in thermal capacity when the glass transition happens. Thus for our photothermal spectroscopy system, we are expected to find the photothermal signal versus QCL drive current curve slope drops down when the glass transition happens. The slope drops down are observed in fig.9 (a)–(d) and fig.10 (a)–(d).

3.3. Photothermal imaging of PMMA USAF target

The USAF target chart is a widely accepted resolution test pattern for optical imaging system. The resolution limitation is defined as the largest line bars that can be resolved by the imaging system. The USAF target has several groups of patterns, each

group has six elements. The resolution limitation for different elements in group 6 and 7 are shown in table 2.

Table 2. The USAF target pattern resolution limitation for different elements in group 6 and 7. The largest line bars that the imaging system can't resolve is the resolution limitation

element	Group 6 resolution(μm)	Group 7 resolution(μm)
1	7.81	3.91
2	6.96	3.48
3	6.2	3.1
4	5.52	2.76
5	4.92	2.46
6	4.38	2.19

When using the photothermal system for imaging, one question is the imaging resolution. Photothermal images on a PMMA USAF target sample are taken to test the resolution limitation of the photothermal imaging system with different QCL drive current, sample z position and time constant. To find the ideal parameter for photothermal imaging, the following steps are done. The QCL drive current is set to 1000mA, the wavenumber is set to 1728cm^{-1} at the PMMA absorption peak. A scan along z axis is done in steps of 5μm to determine the z position with maximum photothermal signal. This z position with the highest photothermal signal is chosen as the starting point for photothermal imaging. The photothermal imaging is taken using a raster scanning mechanism. The minimum step size is 1μm for x and y directions. Each image has a total size of 240μm x 240μm with a step size of 1μm.

To maximize the photothermal imaging resolution, the z position, QCL drive current and the lock-in time constant are varied separately to get the best spatial resolution.

To determine the best parameters for achieving the best imaging resolution for this system, each parameter is varied while keeping the other two parameters constant. For the first study, the z position and lock-in time constant (TC) are fixed to 0.575mm and 71ms, respectively. The QCL drive current is changed from 600mA to 1000mA at a step size of 100mA. The QCL drive current (I1) with the highest spatial resolution is recorded at 1000mA where a resolution of 3.10μm is determined.

For the second study, the QCL drive current and time constant are fixed at 675mA and 71ms, respectively, while the z position is varied by a distance of -10μm and +10μm from z=0.575mm (where the maximum photothermal signal is recorded). The z position with the highest spatial resolution is found to be 0.574mm where a resolution of 2.76μm is determined.

In the third study, both z position and QCL drive current are fixed at 0.574mm and 675mA, respectively. Images were recorded at the different time constants. However, the results are not conclusive because of the experimental recording issues und additional confirmation will be needed.

Photothermal images of USAF target recorded at different QCL drive currents at z=0.575mm, TC=71ms are shown in Fig. 13. Group 7 are shown on the right of the image, the elements 1 to 6 are located from bottom to top. It can be seen that from fig.

13(a)–(d) that element 3 in group 7 can be resolved in all the images. A quantitative analysis of the line scans of each image is conducted to determine the contrast of each image. The images are analyzed by selecting the line scan with the largest photothermal signal dip to peak contrast and averaging it with the two lines adjacent to it. Results of the line scan analysis are shown in Table 3. The contrast is defined as the percent of photothermal signal dip in the maximum signal profile. Since the PMMA USAF target pattern is a negative contrast, the signal profile is defined as the photothermal signal drops below the baseline. The baseline is defined as the photothermal signal at the PMMA films. The results show that the largest contrast is shown for a QCL drive current of 1000mA (shown in fig. 13(e)). Hence, a QCL drive current of 1000mA is determined to be the best QCL current for photothermal imaging.

Table 3. The line scan contrast analysis. The contrast is defined as the ratio between photothermal signal dip and the dip-to-peak value. The best spatial resolution is determined by the Rayleigh criterion. By comparing the minimum contrast, the best QCL current is 1000mA for z=0.575mm, TC=71ms.

QCL current(mA)	Max contrast%	Min contrast%	Smallest elements can be resolved in group 7
1000	40.79	36.30	3
750	37.13	32.21	3
900	39.73	33.66	3
675	32.66	31.78	3

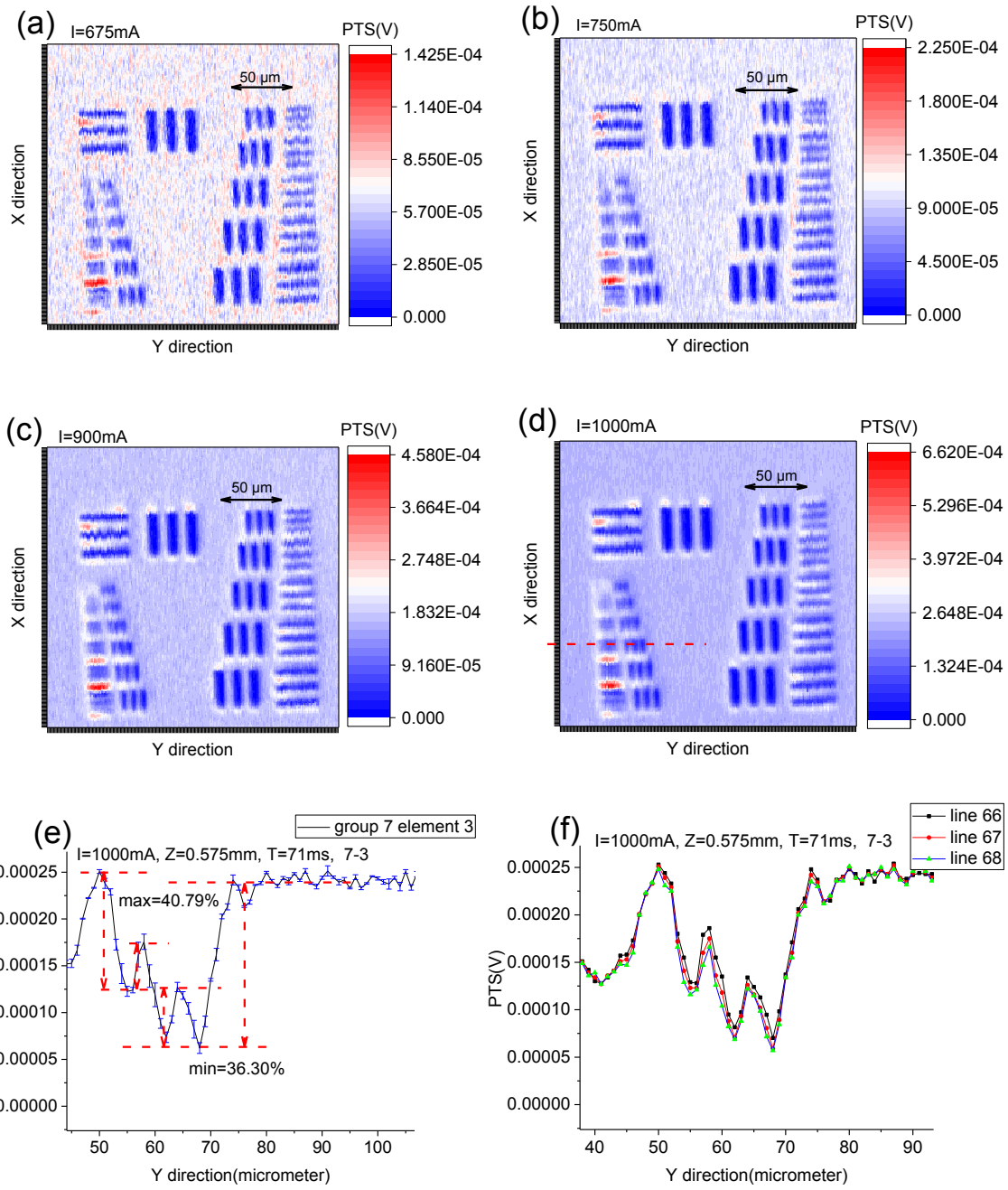

Fig. 13 Photothermal images recorded at a QCL wavenumber of 1728cm^{-1} at different QCL drive currents. The time constant is 71ms and z=0.575mm for all images. The ideal QCL current is 1000mA. (a)-(d) images are taken to find the best QCL drive current. The corresponding QCL drive current is (a) 1000mA; (b) 750mA; (c) 900mA; (d) 675mA. (e) shows the line scan analysis of group 7 element 3 at a QCL drive current=1000mA. The line scan is calculated by averaging three lines at the vicinity of the red dashed line in (d). (f) shows the three lines used for the average in (e). The smallest line bars that can be resolved are group 7 elements 3 for a QCL drive current I=1000mA, z=0.575mm, TC=71ms.

Photothermal images recorded at different z positions are shown fig. 14(a)–(e). A quantitative analysis of the line scan of each image is conducted to determine the contrast of each image. The images are analyzed by selecting the line scan with the largest photothermal signal dip to peak contrast and averaging it with the two (four) lines adjacent to it. Results of the line scan analysis are shown in Table 4. The contrast is defined as the percent of photothermal signal dip in the maximum signal profile, as mentioned before. The resolution is determined by the Rayleigh criterion. Hence, z=0.574mm is determined to be the z position for photothermal imaging. The line scan analysis of I=675mA, z=0.574mm, TC=71ms is shown in fig. 14(f). The z position that results in the best for photothermal imaging resolution is z=0.574mm, the smallest line bars that can be resolved are group 7 element 4, which is corresponding to the line width equals to 2.76μm.

Table 4. The line scan contrast analysis. By comparing the minimum contrast, the best z position is z=0.574mm for I=675mA, T=71ms. The smallest elements can be resolved are group 7 element 4.

Z position (mm)	Max contrast (%)	Min contrast (%)	Smallest elements can be resolved in group 7
0.565	/	/	2
0.569	64.95(averaged by 5 lines) 64.95(averaged by 3 lines)	33.25(averaged by 5 lines) 34.15(averaged by 3 lines)	4
0.571	/	/	2
0.574	61.9(average by 5 lines) 67.31(averaged by 3 lines)	52.34(averaged by 5 lines) 46.52(averaged by 3 lines)	4
0.579	/	/	2

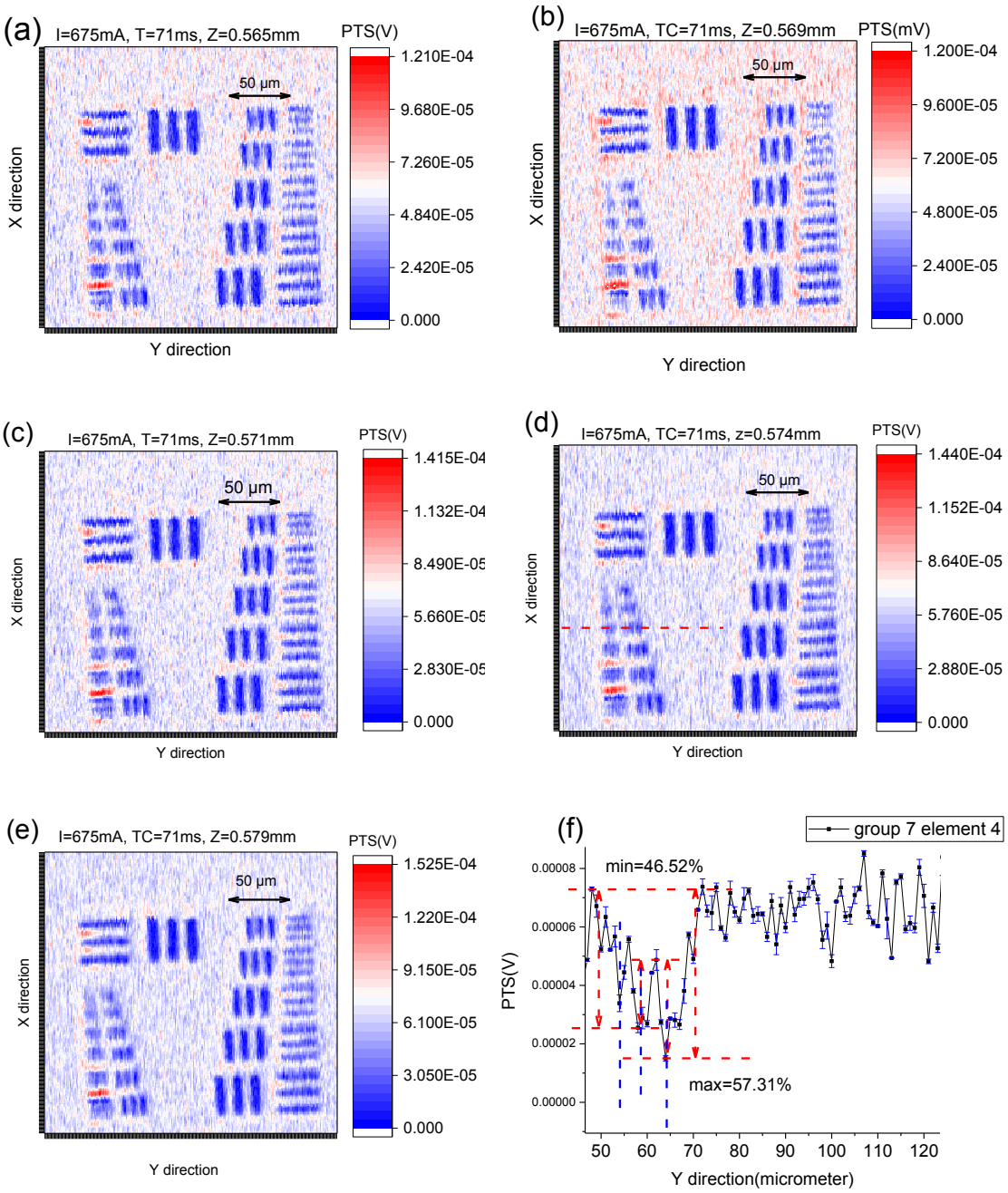
(a)
I=675mA, T=71ms, Z=0.565mm
PTS(V)
1.210E-04
9.680E-05
7.260E-05
4.840E-05
2.420E-05
0.000
50 μm
X direction
Y direction
(b)
I=675mA, TC=71ms, Z=0.569mm
PTS(mV)
1.200E-04
9.600E-05
7.200E-05
4.800E-05
2.400E-05
0.000
50 μm
X direction
Y direction
(c)
I=675mA, T=71ms, Z=0.571mm
PTS(V)
1.415E-04
1.132E-04
8.490E-05
5.660E-05
2.830E-05
0.000
50 μm
X direction
Y direction
(d)
I=675mA, TC=71ms, z=0.574mm
PTS(V)
1.440E-04
1.152E-04
8.640E-05
5.760E-05
2.880E-05
0.000
50 μm
X direction
Y direction
(e)
I=675mA, TC=71ms, Z=0.579mm
PTS(V)
1.525E-04
1.220E-04
9.150E-05
6.100E-05
3.050E-05
0.000
50 μm
X direction
Y direction
(f)
group 7 element 4
min=46.52%
max=57.31%
PTS(V)
0.00008
0.00006
0.00004
0.00002
0.00000
50
60
70
80
90
100
110
120
Y direction(micrometer)

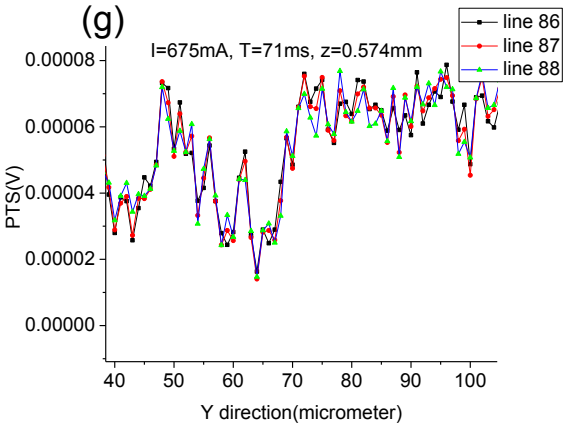

Fig. 14. The photothermal images taken at QCL wavenumber equals to 1728cm^{-1} with different z position. The lock-in time T=71ms and QCL drive current I=675mA. The ideal z position is z=0.574mm. (a)-(e) are imaging taken to find the best QCL drive current. The corresponding z position is (a) 0.565mm; (b) 0.569mm; (c) 0.571mm; (d) 0.574mm; (e) 0.579mm. (f) shows the line scan analysis at z=0.574mm, I=675mA, T=71ms. The line scan is obtained by averaging 3 lines in the vicinity of the red dashed line in (d). These three lines are shown in (g). The smallest line bars that can be resolved are group 7 element 4.

The photothermal images and the optical image of the PMMA USAF target sample are shown in fig. 15. Fig. 15(a) is the photothermal image taken at I=1000mA, z=0.575mm and TC=71ms. Fig.13(b) ishows the photothermal image recorded at I=675mA, z=0.574mm and T=71ms. Fig. 15(c) is the optical image taken by the microscope at x200. Based on the analysis shown in this section, the smallest line bars that can be resolved are group 7 element 4.

The photothermal signal is determined by the spatial overlapping between the probe beam and the pump beam induced thermal lens at the sample plane. For our photothermal imaging system, the diffraction limit spot size for near-infrared beam is ~3.2μm, the mid-infrared beam diffraction limit spot size is ~11.6μm. Since the near-infrared beam diffraction limit spot size is smaller than the mid-infrared diffraction limit spot size, the photothermal imaging system is limited by the probe beam diffraction limit

spot size. The smallest line bars that the photothermal imaging system can resolve are group 7 element 4. The line width of group 7 element 4 is 2.76μm. There are two different definitions for resolving power that links the smallest resolvable line bars and line width with the best spatial resolution the system can achieve. We will discuss these below.

With the first definition, the photothermal imaging can be determined by the distance between the two neighboring photothermal signal dips. The group 7 element 4 line bars in the USAF target have a line width of 2.76μm for a single line. It is close to the diffraction limited spot size of the probe beam. It is reasonable to determine the best spatial resolution by using the distance between two neighboring photothermal signal dips. The Y positions of three photothermal signal dips at group 7 element 4 are Y=54μm, Y=58μm and Y=64μm in fig.12(f). The average distance between the neighboring photothermal signal dips is ~5μm (keeping in mind that our raster scan step size is 1μm). Thus, one conclusion could be that the spatial resolution for the photothermal imaging system is around 5μm, if one assumes the full contrast between individual features. This is by a factor ~ 2 better than diffraction limited spot size of the mid-infrared beam.

With the second definition, the best spatial resolution is determined by the line width of the smallest resolvable line bars. According to this interpretation, the best spatial resolution of the system could be estimated at 2.76μm. However, this value is also better than the near-infrared probe beam diffraction limited spot size. In the following, we discuss a few possible reasons: (1) The PMMA USAF target is a negative contrast

pattern, at the edge of PMMA pattern area, edge effects can increase the photothermal signal sharpness at the PMMA film area, which can enhance resolution. (2) The photothermal signal is determined by the spatial overlap between the near-infrared probe beam and the thermal lens induced by pump beam at the sample plane. If the probe beam is only partially overlapping the thermal lens at the sample plane, that might lead to a higher spatial resolution. (3) The exact pattern of the PMMA USAF target needs to be remeasured after the photothermal analysis to confirm that the design line widths are maintained as fabrication uncertainties can lead to slightly larger/smaller feature sizes.

Thus, future experiments that identify a point spread function will be important for a conclusive result.

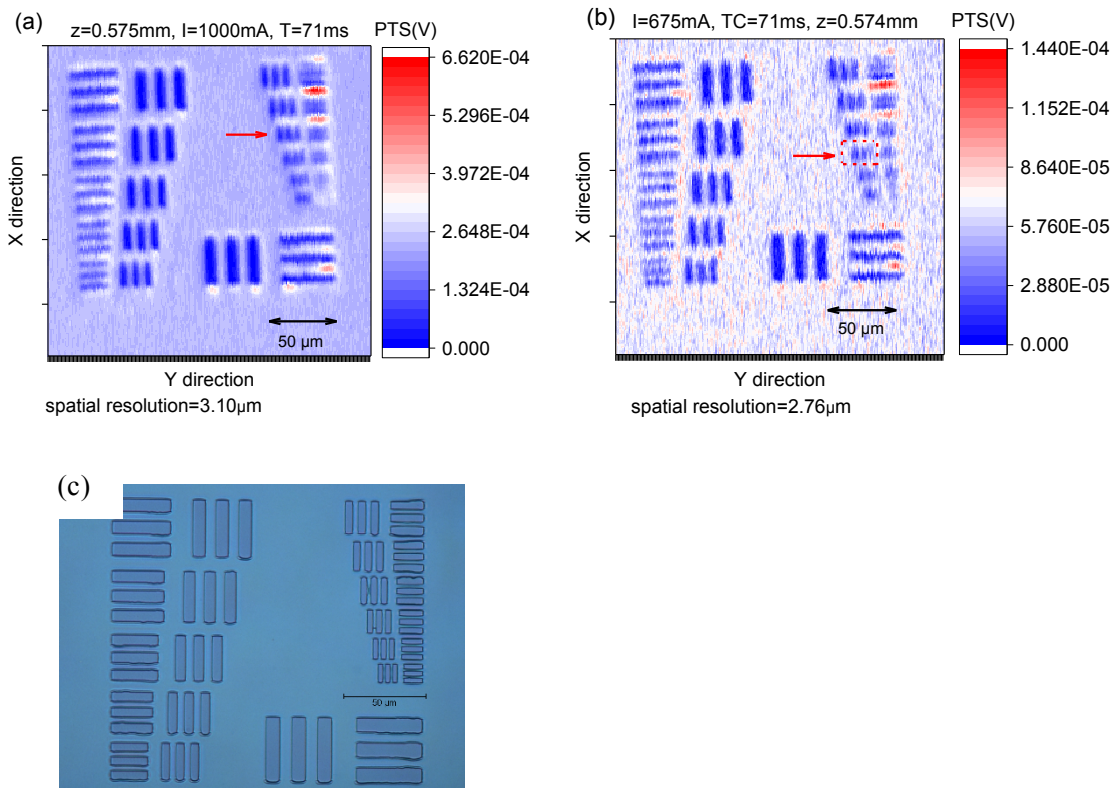

Fig. 15. Photothermal images and the optical image of the PMMA USAF target sample. (a) is the photothermal image taken at QCL I=1000mA, z=0.575mm and T=71ms; The smallest line bars that can be resolved are group 7 element 3, which has a line width of 3.10μm for a single line. (b) photothermal image taken with I=675mA, z=0.574mm and T=71ms. The smallest line bars can be resolved are group 7 element 4, which has a line width of 2.76μm for a single line. (c) Optical image taken at 200x magnification. The smallest line bars that can be resolved by the photothermal imaging system is group 7 element 4, which is shown in the red dashed line box in (b). Which corresponding to a spatial resolution equal to 5μm according to definition (1), 2.76μm according to definition (2).

References

[1] Power, Joan F. “Pulsed mode thermal lens effect detection in the near field via thermally induced probe beam spatial phase modulation: a theory.” *Applied Optics* 29.1 (1990): 52–63.

[2] Gaiduk, A., et al. “Room-temperature detection of a single molecule’s absorption by photothermal contrast.” *Science* 330.6002 (2010): 353–356.

[3] Cognet, Laurent, et al. “Single metallic nanoparticle imaging for protein detection in cells.” *Proceedings of the National Academy of Sciences of the United States of America* 100.20 (2003): 11350–11355.

[4] He, Jinping, et al. “Label-free imaging of melanoma with nonlinear photothermal microscopy.” *Optics Letters* 40.7 (2015): 1141–1144.

[5]. Pfeifer, Marcel, Alexander Ruf, and Peer Fischer. “Indirect absorption spectroscopy using quantum cascade lasers: mid-infrared refractometry and photothermal spectroscopy.” *Optics Express* 21.22 (2013): 25643–25654.

[6] Anderson, Rosaleen J., David J. Bendell, and Paul W. Groundwater. *Organic Spectroscopic Analysis*. Vol. 22 of *Tutorial Chemistry Texts*. Cambridge: Royal Society of Chemistry, 2004.

[7] Griffiths, Peter R., and James A. De Haseth. *Fourier Transform Infrared Spectrometry*. 2nd edition. Hoboken, NJ: Wiley Interscience, 2007.

[8] Mërtiri, Alket, et al. “Mid-infrared photothermal heterodyne spectroscopy in a liquid crystal using a quantum cascade laser.” *Applied Physics Letters* 101.4 (2012): 044101.

[9] Farahi, R. H., et al. “Pump–probe photothermal spectroscopy using quantum cascade lasers.” *Journal of Physics D: Applied Physics* 45.12 (2012): 125101.

[10] Totachawattana, Atcha, et al. “Vibrational mid-infrared photothermal spectroscopy using a fiber laser probe: asymptotic limit in signal-to-baseline contrast.” *Optics Letters* 41.1 (2016): 179–182.

[11] Yeh, Kevin, et al. “Fast infrared chemical imaging with a quantum cascade laser.” *Analytical Chemistry* 87.1 (2014): 485–493.

[12] Totachawattana, Atcha, Shyamsunder Erramilli, and Michelle Y. Sander. “Optimization of mid-IR photothermal imaging for tissue analysis.” *Proceedings of SPIE* 9584, Ultrafast Nonlinear Imaging and Spectroscopy III, 95840C (August 26, 2015); doi:10.1117/12.2187652.

[13] Furstenberg, Robert, et al. "Chemical imaging using infrared photothermal microspectroscopy." *Proceedings of SPIE* 8374, Next-Generation Spectroscopic Technologies V, 837411 (18 May 2012); doi: 10.1117/12.919574

[14] Zhang, Delong, et al. "Depth-resolved mid-infrared photothermal imaging of living cells and organisms with submicrometer spatial resolution." *Science Advances* 2.9 (2016): e1600521.

[15] Li, Zhongming, Masaru Kuno, and Gregory Hartland. "Super-resolution imaging with mid-IR photothermal microscopy on the single particle level." *Proceedings of SPIE* 9549, Physical Chemistry of Interfaces and Nanomaterials XIV, 954912 (20 August 2015); doi: 10.1117/12.2188337

[16] Schild, Howard G. "Poly (N-isopropylacrylamide): experiment, theory and application." *Progress in Polymer Science* 17.2 (1992): 163–249.

[17] Huber, Dale L., et al. "Programmed adsorption and release of proteins in a microfluidic device." *Science* 301.5631 (2003): 352–354.

[18] Wichterle, O., and D. Lim. "Hydrophilic gels for biological use." *Nature* 185.4706 (1960): 117–118.

[19] Gupta, Piyush, Kavita Vermani, and Sanjay Garg. "Hydrogels: from controlled release to pH-responsive drug delivery." *Drug Discovery Today* 7.10 (2002): 569–579.

[20] Arshady, Reza. "Functional monomers." *Journal of Macromolecular Science, Part C: Polymer Reviews* 32.1 (1992): 101–132.

[21] Meakin, J. R., et al. "Thermal analysis of poly (2-hydroxyethyl methacrylate)(pHEMA) hydrogels." *Journal of Materials Science: Materials in Medicine* 14.1 (2003): 9–15.

[22] Morita, Shigeaki. "Hydrogen-bonds structure in poly (2-hydroxyethyl methacrylate) studied by temperature-dependent infrared spectroscopy." *Frontiers in Chemistry* 2 (2014): 10.

[23] Zhou, Yingshan, et al. "A pH-sensitive water-soluble N-carboxyethyl chitosan/poly (hydroxyethyl methacrylate) hydrogel as a potential drug sustained release matrix prepared by photopolymerization technique." *Polymers for Advanced Technologies* 19.8 (2008): 1133–1141.

[24] Furstenberg, Robert, et al. "Stand-off detection of trace explosives via resonant infrared photothermal imaging." *Applied Physics Letters* 93.22 (2008): 224103

[25] Morita, Shigeaki. “Hydrogen-bonds structure in poly (2-hydroxyethyl methacrylate) studied by temperature-dependent infrared spectroscopy.” *Frontiers in Chemistry* 2 (2014): 10.

[26] Bolbukh, Yuliia, et al. “Glass transition and hydration properties of polyhydroxyethylmethacrylate filled with modified silica nanoparticles.” *Journal of Thermal Analysis and Calorimetry* 125.3 (2016): 1387–1398.

[27] Perova, T. S., J. K. Vij, and H. Xu. “Fourier transform infrared study of poly (2-hydroxyethyl methacrylate) PHEMA.” *Colloid & Polymer Science* 275.4 (1997): 323–332.

Curriculum Vitae